Spatial Aspects of Homonuclear, Proton NMR Cross-Relaxation. 1. The Effects of Molecular Shape and Internal Motion

Anthony J. Duben† and William C. Hutton*

Contribution from the Computer Science Department, Southeast Missouri State University, 1 University Plaza, Cape Girardeau, Missouri 63701, and Monsanto Corporate Research, Physical Sciences Center, Monsanto Company, 700 Chesterfield Village Parkway, St. Louis, Missouri 63198. *Received January 10, 1990*

Abstract: A detailed theoretical analysis of longitudinal NMR cross-relaxation for a proton pair attached to molecules with a variety of sizes and shapes is presented. The universally applied rigid isotropic model for calculating cross-relaxation behavior has been extended to treat a rotating proton pair on a spherical molecule and on prolate and oblate ellipsoids and a rigid proton pair on prolate and oblate ellipsoids. The nuclear Overhauser effect enhancement and the time dependence of two-dimensional NMR cross-peak intensity are calculated and compared to the simpler rigid isotropic case. When internal rotation is considered, it is shown that the nuclear Overhauser enhancement depends on the spatial aspects of the proton pair's motion. Likewise, the initial slope of the cross-peak evolution is a function of not only the internuclear distance but also the geometrical orientation of the proton pair and of rates of global and internal rotation as well. These results differ significantly with use of the rigid isotropic model. When the spatial aspects of motional averaging and internal rotation are ignored, calculated proton internuclear distances can be overestimated by up to 300%. The classification of cross-relaxation being either in spin-diffusion or extreme-narrowing conditions does not necessarily characterize the rotational motion of the molecule as a whole if more than one rotational correlation time is included in the spectral density terms. Rigid protons in macromolecules such as proteins and small DNA/RNA segments are least sensitive to geometric factors. When internal motion or highly anisotropic global molecular motion is present, accurate interpretation and simulation of cross-relaxation behavior requires the full form of the spectral density functions described here.

Introduction

NMR studies of longitudinal cross-relaxation among protons are widely used to determine proton–proton internuclear distances in organic molecules,[1] natural products,[2] peptides and proteins,[3] DNA/RNA fragments,[4] and oligosaccharides.[5] With smaller molecules, the degree of cross-relaxation measured by either one-dimensional or two-dimensional experiments is most often used qualitatively to distinguish between structural candidates. Qualitative characterization of cross-relaxation in biomacromolecules has also proven to be useful. A large number of qualitative distance constraints (usually simply classified as strong, medium, and weak) form the basis for computational methods used to construct three-dimensional structures.[6] The time evolution of cross-relaxation in biomacromolecules can also be followed quantitatively.[7] Buildup rates for cross-relaxation are used to calculate upper bounds on distances between pairs of protons. Either the initial slope or a full relaxation matrix analysis of the cross-peak time dependence is used to establish distance constraints. Often the cross-peak evolution of a proton pair with a known internuclear distance (e.g. a methylene group) is used to calibrate the distances for all of the other proton pairs of interest.

Recently it has become desirable to check the validity of proposed molecular structure(s) by calculating NMR cross-relaxation spectra from the predicted proton–proton distances. The NMR experiment is not subject to any assumptions or restrictions and quantitative simulations of relaxation spectra will only succeed when the underlying theory is complete. The rigid isotropic model of motional averaging is universally employed in homonuclear cross-relaxation experiments. In this model it is assumed that the overall molecular shape has spherical symmetry and internal motion of the interacting protons can safely be ignored.[7,8] Any differences in the motional averaging for proton pairs in the molecule are not considered. Modulation of the internuclear vector between the proton pairs by internal rotation is described only by a single correlation time. The simple relationships that result indicate that, for a given correlation time, the internuclear distance will always be the dominant factor in the cross-relaxation equations. Distance constraints calculated by using the simplified expressions have clearly been successful, particularly when applied to rigid networks of protons such as those found in the peptide backbones of proteins. However, no rigorous theoretical examination of the conditions where the rigid isotropic model is valid has been made. As the quality of the experimental data improves, it is important to carefully examine this model and, if necessary, to expand cross-relaxation theory.

Many macromolecules (large proteins, DNA/RNA fragments, oligosaccharides, phospholipids, micelles, and semiflexible polymers) deviate significantly from spherical symmetry. Practically all macromolecules have regions with heterogeneous internal motion. Because cross-relaxation is one of the most powerful methods for elucidating molecular structure, it is desirable to define the conditions where the rigid isotropic model can safely be applied. In this paper we investigate the importance of anisotropic molecular tumbling and internal rotation in the interpretation and

* Address correspondence to this author at Monsanto Company.
† Southeast Missouri State University.

(1) Sanders, J. K. M.; Mersh, J. D. *Prog. NMR Spectrosc.* **1982**, *15*, 353. Neuhaus, D.; Williamson, M. P. *The Nuclear Overhauser Effect in Structural and Conformational Analysis*; Verlag Chemie: New York, 1988.
(2) Hall, L. D.; Sanders, J. K. M. *J. Am. Chem. Soc.* **1980**, *102*, 5703. Hutton, W. C.; Graden, D. W.; Lynn, D. L. *J. Chem. Soc., Chem. Commun.* **1983**, 864.
(3) Heald, S. L.; Mueller, L.; Jeffs, P. W. *J. Magn. Reson.* **1987**, *72*, 120. Lautz, J.; Kessler, H.; Blaney, J. M.; Scheek, R. M.; van Grunsteren, W. F. *Int. J. Peptide Protein Res.* **1989**, *33*, 281. Wüthrich, K. *NMR of Proteins and Nucleic Acids*; Wiley: New York, 1986.
(4) Wemmer, D. E.; Reid, B. R. *Annu. Rev. Phys. Chem.* **1985**, *36*, 105. Broido, M. S.; James, T. L.; Zon, G.; Keepers, J. W. *Eur. J. Biochem.* **1985**, 117. Wemmer, D. E.; Kim, S. H. *Science* **1987**, *238*, 1722. Kaptein, R.; Boelens, R.; Scheek, R. M.; Van Grunsteren, W. F. *Biochemistry* **1988**, *27*, 5389.
(5) Brisson, J.-R.; Carver, J. P. *Biochemistry* **1983**, *22*, 3689. Homans, S. W.; Dwek, R. A.; Rademacher, T. W. *Biochemistry* **1987**, *262*, 6571.
(6) Kumar, A.; Wagner, G.; Ernst, R. R.; Wüthrich, K. *J. Am. Chem. Soc.* **1981**, *103*, 3654. Clore, G. M.; Gronenborn, A. M.; Mogens, K.; Poulson, F. M. *Protein Eng.* **1987**, *1*, 305. Lee, M. S.; Gippert, G. P.; Kizhake, V. S.; Case, D. A.; Wright, P. E. *Science* **1989**, *245*, 635.
(7) Massefski, W., Jr.; Bolton, P. H. *J. Magn. Reson.* **1985**, *65*, 526. Borgias, B. A.; James, T. L. *Methods Enzymol.* **1989**, *176*, 169. Clore, G. M.; Gronenborn, A. M. *J. Magn. Reson.* **1989**, *84*, 398.
(8) Noggle, J. H.; Schirmer, R. E. *The Nuclear Overhauser Effect: Chemical Applications*; Academic Press: New York, 1971.

0002-7863/90/1512-5917$02.50/0

simulation of cross-relaxation phenomena.

Theory

Woessner and co-workers developed a theory to describe autocorrelated relaxation in ellipsoids for proton pairs with and without internal motion.[9,10] In this treatment the major axis of the ellipsoid rotates with a correlation time τ_1, and τ_2 is the correlation time about the minor axis. The proton pair rotates freely with correlation time τ_r about an axis at angle α with respect to the major axis of the ellipsoid. The internuclear vector between the two protons subtends an angle Δ with respect to the axis of its rotation (see Figure 3a). The formulae developed for this system were used to calculate T_1 and T_2 relaxation rates. They have been applied infrequently because of their relative complexity and because it is difficult to experimentally determine the relevant rotational correlation times. Nonetheless, applying Woessner's results to proton cross-relaxation is a practical starting point for expanding the quantitative utility of one-dimensional and two-dimensional cross-relaxation experiments. Our results indicate that molecular shape and internal motion can have a significant effect on the intensity and time dependence of cross-relaxation. For a fixed set of global correlation times, the internuclear distance will not always be the dominant factor governing cross-relaxation.

Longitudinal relaxation spectral density functions are the building blocks of relaxation calculations. If the proton pair spins freely, the formula for the autocorrelated spectral density functions is given by

$$J_n(\omega) = K_n[B_A f_n(\tau_{A1}) + B_{A2} f_n(\tau_{A2}) + B_{A3} f_n(\tau_{A3}) + B_B f_n(\tau_{B1}) + B_{B2} f_n(\tau_{B2}) + B_{B3} f_n(\tau_{B3}) + B_C f_n(\tau_{C1}) + B_{C2} f_n(\tau_{C2}) + B_{C3} f_n(\tau_{C3})] \quad (1)$$

where $K_n = {}^4/_5$, ${}^2/_{15}$, and ${}^8/_{15}$ for $n = 0$, 1, and 2, respectively. The form of the spectral density functions, J_n, used in (1) is that used by Woessner.[9,10] Their relationship to other commonly encountered forms of the spectral density functions can be found in the Appendix included in the supplementary material. Equation 1 is the complete expression for the spectral density functions for the general case of a nonspherical ellipsoid with unhindered internal motion. No simplifying assumptions or restrictions are imposed.

The B_A, B_B, and B_C coefficients in eq 1 reflect the spatial aspects of the tensor operators responsible for the relaxation of longitudinal magnetization. Their complete form is given in eq A2a–A2i in the Appendix (supplementary material) and in the original references.[9,10] The terms in the B_A, B_B, and B_C coefficients are related to the symmetry properties of second rank spherical harmonics.[12]

The $f_n(\tau_i)$ terms in (1) can be written as

$$f_n(\tau_i) = \frac{\tau_i}{1 + (n\omega\tau_i)^2} \quad (n = 0, 1, 2) \quad (2)$$

where τ_i represents the expressions for the nine effective correlation times, τ_{A1}–τ_{C3}, required to describe free rotation of a proton pair attached to an ellipsoid-shaped molecule. The τ_i terms are composed of ratios of products and sums of τ_1, τ_2, and τ_r. The complete expressions for the τ_{A1}–τ_{C3} correlation times are given in the Appendix (supplementary material) and in the original references.[9,10]

The nuclear Overhauser effect enhancement, η, with the values for J_n given in eq 1 is

$$\eta = -\frac{J_0 - 9J_2}{J_0 + 18J_1 + 9J_2 + (4R_s/5\pi q)} \quad (3)$$

where R_s is the rate of relaxation due to sources other than the dipole–dipole relaxation between the two protons and q is the collection of values $q = (1/10)(\gamma_H{}^4\hbar^2/r^6)$ and r is the distance between the protons. The values for η described in eq 3 are based on the steady-state, presaturation technique. Similar results hold for the exchange of longitudinal magnetization through cross-relaxation as measured in homonuclear, two-dimensional experiments (NOESY).[13,14] For a proton pair, simple substitution of the formulae in ref 14 shows that in two-dimensional spectra the ratio of cross-peak to diagonal-peak intensity at the optimum mixing time is $-\eta$, as calculated here.

The time evolution of the cross-peak intensity in a two-dimensional cross-relaxation study can be calculated by substitution of the complete spectral densities described in eq 1 into the equations in ref 14. The rate of change of cross-peak intensity, I_{AB}, with respect to mixing time, t_m, for cross-relaxation between two protons A and B is[14]

$$\frac{dI_{AB}}{dt_m} = -(M_0/4)\frac{(9J_2 - J_0)}{|(9J_2 - J_0)|}[(R_C + R_L)(\exp(-R_C t_m)) - R_L \exp(-R_L t_m)] \quad (4)$$

where M_0 is the equilibrium Z magnetization; R_C contains the cross-relaxation terms; and R_L contains the leakage relaxation terms. The expressions used in eq 4 are defined in an Appendix in the supplementary material.

The calculation of either η or cross-peak evolution including the effects of molecular shape and the orientation of a proton pair undergoing internal motion can be done with eqs 3 or 4. There are three general cases where molecular symmetry and/or lack of internal motion simplify the expressions in eq 1.

A sphere without internal motion is the frequently used rigid isotropic model. The standard equations applied in this model can be derived by using spectral density functions calculated from eq 1 with $\tau_1 = \tau_2 = \tau_c$ and $\tau_c \ll \tau_r$.[8] As τ_c increases, η changes from positive to negative values, illustrating the change from above to below extreme-narrowing conditions. Since the molecule is spherical and there is no internal motion, the placement of the protons is irrelevant.

When the sphere has a rotating proton pair, $\tau_1 = \tau_2 = \tau_c$, only functions in Δ survive in the angular factors. The complete equations for J_n and the expressions for the required correlation times are found in the Appendix (supplementary material).

When $\tau_1 \neq \tau_2$ but $\tau_r \gg \tau_1, \tau_2$, we have an ellipsoid in which the protons are effectively fixed as the molecule tumbles. The spectral density functions, J_n, become

$$J_n = (K_n/2)\left[(1 - 3\cos^2\Delta)^2 f_n(\tau_2) + 3[\sin^2(2\Delta)]f_n\left(\frac{6\tau_1\tau_2}{5\tau_1 + \tau_2}\right) + 3(\sin^4\Delta)f_n\left(\frac{6\tau_1\tau_2}{2\tau_1 + 4\tau_2}\right)\right] \quad (5)$$

The only angle involved in eq 5 is Δ (the angle that the internuclear vector makes with the major axis of the ellipsoid). The proton pair assumes all possible orientations as the molecule tumbles. In deriving eq 5 the fundamental correlation function, $\langle F_n(t)F_n(t + t')\rangle$, was integrated to evaluate Woessner's spectral density equations.[9] Functions over the angle α generate ($\sin^2\alpha + \cos^2\alpha$) terms that are always unity, thereby removing any angular dependence on α. Choosing, for convenience, a value of 0 for α allows us to associate the angle Δ in Figure 3a with the terms containing Δ that appear in eq 5.

Results

In order to investigate the effects of molecular symmetry and internal rotation on cross-relaxation, eq 3 and 4 were used to calculate the η and cross-peak evolution for a number of situations often encountered in NMR studies. The results for a spectrometer frequency of 500 MHz, an internuclear distance of 3.46 Å, and $R_s = 0$ are listed in Tables I–III and are graphically depicted in

(9) Woessner, D. E. *J. Chem. Phys.* **1962**, *37*, 647.
(10) Woessner, D. E.; Snowden, B. S., Jr.; Meyer, G. H. *J. Chem. Phys.* **1969**, *50*, 719.
(11) Werbelow, L. G. *J. Am. Chem. Soc.* **1978**, *100*, 7095.
(12) Sanctuary, B. S.; Selwyn, L. J. *Chem. Phys.* **1981**, *74*, 906. Halstead, T. K.; Osmet, P. A.; Sanctuary, B. S. *J. Magn. Reson.* **1984**, *60*, 382.
(13) Jeener, J.; Meier, B. H.; Bachmann, P.; Ernst, R. R. *J. Chem. Phys.* **1979**, *71*, 4546.
(14) Macura, S.; Ernst, R. R. *Mol. Phys.* **1980**, *41*, 95.

Table I. Nuclear Overhauser Effect Enhancements and Calculated Interproton Distances for a Rotating Proton Pair Attached to a Sphere[a]

τ_c	τ_r	Δ	η	r (% error)[b]
1×10^{-12}	1×10^{-12}	0	0.50	3.46 (0)
		30	0.50	3.69 (7)
		60	0.50	4.06 (17)
		90	0.50	4.03 (17)
1×10^{-9}	1×10^{-12}	0	−0.60	3.46 (0)
		30	−0.59	4.05 (17)
		60	−0.34	7.26 (110)
		90	−0.59	4.36 (26)
1×10^{-9}	1×10^{-9}	0	−0.60	3.46 (0)
		30	−0.35	3.85 (11)
		60	−0.02	6.14 (77)
		90	−0.01	6.86 (98)
1×10^{-6}	1×10^{-12}	0	−1	3.46 (0)
		30	−1	4.05 (17)
		60	−1	6.92 (100)
		90	−1	4.36 (26)
1×10^{-6}	1×10^{-9}	0	−1	3.46 (0)
		30	−1	4.05 (17)
		60	−0.95	6.89 (99)
		90	−1	4.36 (26)

[a] Other fixed parameters for this calculation are the following: $\omega = 2\pi \times 500$ MHz, $R_s = 0$. [b] r is in Å. Deviation from the distance calculated by using the rigid isotropic model ($r = 3.46$ Å).

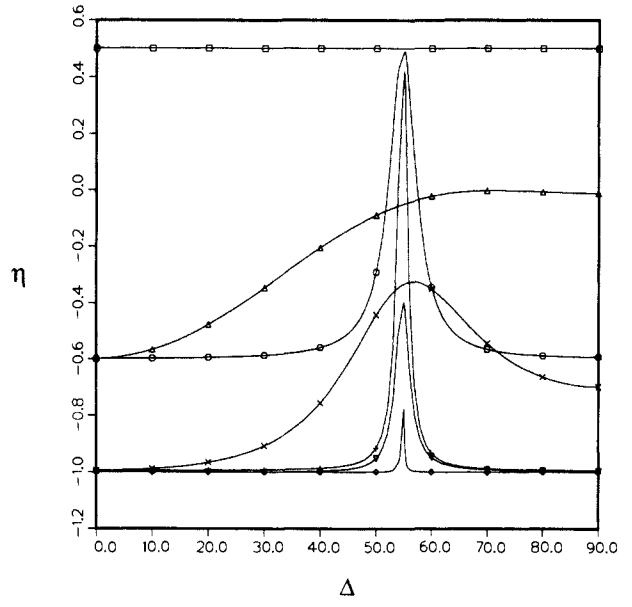

Figure 1. NOE enhancements, η, as a function of the angle Δ for a rotating proton pair attached to a sphere: (□) $\tau_c = 1 \times 10^{-12}$, $\tau_r = 1 \times 10^{-12}$; (○) $\tau_c = 1 \times 10^{-9}$, $\tau_r = 1 \times 10^{-12}$; (△) $\tau_c = 1 \times 10^{-9}$, $\tau_r = 1 \times 10^{-9}$; (+) $\tau_c = 1 \times 10^{-8}$, $\tau_r = 1 \times 10^{-12}$; (×) $\tau_c = 1 \times 10^{-8}$, $\tau_r = 1 \times 10^{-9}$; (◇) $\tau_c = 1 \times 10^{-6}$, $\tau_r = 1 \times 10^{-12}$; (▽) $\tau_c = 1 \times 10^{-6}$, $\tau_r = 1 \times 10^{-9}$.

Figures 1–5. Given a molecule with τ_1 and τ_2, a pair of protons at internuclear distance r moving with internal correlation time τ_r, the η or cross-peak evolution for the protons as a function of α and Δ can be read from the plots. The tables contain the calculated value for r that would result from assuming the rigid isotropic model. When α and/or Δ are equal to 0 the result is identical with that obtained with use of the rigid isotropic spectral densities. The calculations reveal that there are a wide variety of cases where both η and slope are sensitive to the overall shape of the molecule, to the orientation of the protons in the molecule, and to the rate of internal motional averaging. The error in determining the interproton distance, as determined from the initial slope of the cross-peak buildup curves, can also be found in the tables. The error represents the amount the distance is miscalculated when the simple, rigid isotropic model is applied.

Case 1: Ellipsoids with Internal Rotation. The spectral density functions for an ellipsoid with internal rotation are given by eq 1 and the related equations in the Appendix (supplementary material). The simplest ellipsoid is a sphere, the approximate shape of many biomacromolecules. This case has been treated in the literature[11] and was recently extended to systems where significant external relaxation (paramagnetic metal) is present.[15] In contrast to the earlier treatments, here we choose to keep the correlation times τ_c and τ_r fixed and evaluate the cross-relaxation as a function of the angle for internal motion. Figure 1 shows the angular dependence of η for a spherical molecule with an attached proton pair rotating about Δ. When internal rotation is considered, η can depend strongly on the orientation of the pair even for isotropic global motion. Parts a and b of Figure 2 depict the cross-peak evolution for spherical molecules with a rotating pair. The rates of growth of cross-peak intensity are clearly dependent on Δ. When τ_c is well into the spin-diffusion regime (Figure 2a) the initial slope is linear only at very short mixing times. With shorter correlation times (Figure 2b) the initial growth of the intensities as a function of time is linear. The slopes are dependent on Δ in spite of the fact that both τ_c and τ_r were set to 1×10^{-9} s. Similar results were obtained for $\tau_c = 1 \times 10^{-8}$ (supplementary material). The variation in the slopes is due to the B_A, B_B, and B_C terms in eq 1. Table I summarizes the in-

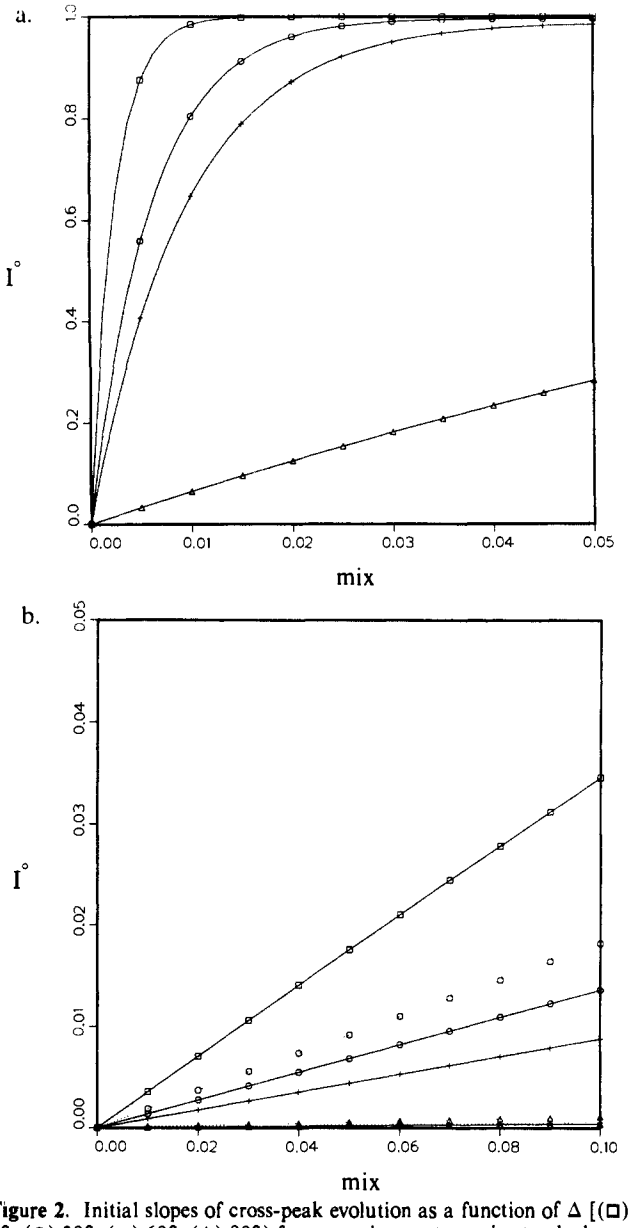

Figure 2. Initial slopes of cross-peak evolution as a function of Δ [(□) 0°, (○) 30°, (△) 60°, (+) 90°) for a rotating proton pair attached to a sphere: (a) (—) $\tau_c = 1 \times 10^{-6}$, $\tau_r = 1 \times 10^{-9}$; (b) (—) $\tau_c = 1 \times 10^{-9}$, $\tau_r = 1 \times 10^{-12}$; (···) $\tau_c = 1 \times 10^{-9}$, $\tau_r = 1 \times 10^{-9}$.

(15) Duben, A. J.; Hutton, W. C. *J. Magn. Reson.* **1990**, *88*, 60.

Table II. Nuclear Overhauser Effect Enhancements and Calculated Interproton Distances for a Rotating Proton Pair Attached to Prolate Ellipsoids[a]

		Δ						Δ		
	α	0	30	60	90	α	0	30	60	90
				$\tau_1 = 5 \times 10^{-13}$; $\tau_2 = 1 \times 10^{-12}$; $\tau_r = 1 \times 10^{-12}$						
η	0	0.50	0.50	0.50	0.50	60	0.50	0.50	0.50	0.50
r (% error[b])		3.46 (0)	3.71 (7)	4.12 (19)	4.06 (17)		3.63 (5)	3.83 (11)	4.15 (20)	4.16 (20)
η	30	0.50	0.50	0.50	0.50	90	0.50	0.50	0.50	0.50
r (% error[b])		3.52 (2)	3.75 (8)	4.13 (19)	4.10 (19)		3.67 (6)	3.86 (12)	4.17 (20)	4.18 (21)
				$\tau_1 = 5 \times 10^{-10}$; $\tau_2 = 1 \times 10^{-9}$; $\tau_r = 1 \times 10^{-12}$						
η	0	−0.60	−0.59	−0.34	−0.59	60	−0.43	−0.42	−0.20	−0.42
r (% error[b])		3.46 (0)	4.05 (17)	7.26 (110)	4.36 (26)		3.72 (7)	4.36 (26)	8.07 (133)	4.69 (36)
η	30	−0.54	−0.53	−0.29	−0.53	90	−0.38	−0.37	−0.16	−0.37
r (% error[b])		3.55 (2)	4.15 (20)	7.51 (117)	4.47 (29)		3.80 (10)	4.46 (29)	8.37 (142)	4.79 (39)
				$\tau_1 = 5 \times 10^{-10}$; $\tau_2 = 1 \times 10^{-9}$; $\tau_r = 1 \times 10^{-9}$						
η	0	−0.60	−0.32	0.02	0.01	60	−0.43	−0.22	0.04	0.06
r (% error[b])		3.46 (0)	3.90 (13)	c	c		3.72 (7)	4.19 (21)	c	c
η	30	−0.54	−0.29	0.02	0.03	90	−0.38	−0.19	0.04	0.07
r (% error[b])		3.55 (2)	3.99 (15)	c	c		3.80 (10)	4.30 (24)	c	c
				$\tau_1 = 5 \times 10^{-9}$; $\tau_2 = 1 \times 10^{-8}$; $\tau_r = 1 \times 10^{-12}$						
η	0	−0.99	−0.99	−0.93	−0.99	60	−0.99	−0.99	−0.91	−0.99
r (% error[b])		3.46 (0)	4.05 (17)	6.94 (101)	4.36 (26)		3.63 (5)	4.25 (23)	7.30 (111)	4.57 (32)
η	30	−0.99	−0.99	−0.93	−0.99	90	−0.99	−0.98	−0.90	−0.99
r (% error[b])		3.52 (2)	4.12 (19)	7.07 (104)	4.44 (28)		3.67 (6)	4.30 (24)	7.38 (113)	4.63 (34)
				$\tau_1 = 5 \times 10^{-9}$; $\tau_2 = 1 \times 10^{-8}$; $\tau_r = 1 \times 10^{-9}$						
η	0	−0.99	−0.91	−0.34	−0.70	60	−0.99	−0.88	−0.32	−0.63
r (% error[b])		3.46 (0)	3.98 (15)	5.73 (66)	4.40 (27)		3.63 (5)	4.16 (20)	5.83 (69)	4.64 (34)
η	30	−0.99	−0.90	−0.34	−0.67	90	−0.99	−0.87	−0.31	−0.61
r (% error[b])		3.52 (2)	4.04 (17)	5.77 (67)	4.49 (30)		3.67 (6)	4.20 (21)	5.85 (69)	4.70 (36)
				$\tau_1 = 5 \times 10^{-7}$; $\tau_2 = 1 \times 10^{-6}$; $\tau_r = 1 \times 10^{-12}$						
η	0	−1.0	−1.0	−1.0	−1.0	60	−1.0	−1.0	−1.0	−1.0
r (% error[b])		3.46 (0)	4.05 (17)	6.92 (100)	4.36 (26)		3.63 (5)	4.24 (23)	7.26 (110)	4.57 (32)
η	30	−1.0	−1.0	−1.0	−1.0	90	−1.0	−1.0	−1.0	−1.0
r (% error[b])		3.52 (2)	4.12 (19)	7.04 (103)	4.44 (28)		3.67 (6)	4.29 (24)	7.34 (112)	4.63 (34)
				$\tau_1 = 5 \times 10^{-7}$; $\tau_2 = 1 \times 10^{-6}$; $\tau_r = 1 \times 10^{-9}$						
η	0	−1.0	−1.0	−0.95	−1.0	60	−1.0	−1.0	−0.93	−0.99
r (% error[b])		3.46 (0)	4.05 (17)	6.89 (99)	4.36 (26)		3.63 (5)	4.24 (23)	7.22 (109)	4.57 (32)
η	30	−1.0	−1.0	−0.94	−1.0	90	−1.0	−1.0	−0.93	−0.99
r (% error[b])		3.52 (2)	4.12 (19)	7.01 (103)	4.44 (28)		3.67 (6)	4.29 (24)	7.30 (111)	4.63 (34)
				$\tau_1 = 10^{-9}$; $\tau_2 = 1 \times 10^{-6}$; $\tau_r = 1 \times 10^{-12}$						
η	0	−1.0	−1.0	−1.0	−1.0	60	−0.99	−0.99	−0.96	−0.99
r (% error[b])		3.46 (0)	4.05 (17)	6.92 (100)	4.36 (26)		6.67 (93)	7.80 (125)	13.36 (286)	8.40 (143)
η	30	−1.0	−1.0	−1.0	−1.0	90	−1.0	−1.0	−1.0	−1.0
r (% error[b])		4.04 (17)	4.73 (37)	8.08 (134)	5.09 (47)		4.36 (26)	5.10 (47)	8.71 (152)	5.49 (59)
				$\tau_1 = 10^{-9}$; $\tau_2 = 1 \times 10^{-6}$; $\tau_r = 1 \times 10^{-9}$						
η	0	−1.0	−1.0	−0.94	−1.0	60	−0.99	−0.93	−0.36	−0.82
r (% error[b])		3.46 (0)	4.05 (17)	6.90 (99)	4.36 (26)		6.67 (93)	7.74 (124)	12.11 (250)	8.44 (144)
η	30	−1.0	−1.0	−0.87	−0.99	90	−1.0	−0.99	−0.81	−0.98
r (% error[b])		4.04 (17)	4.72 (37)	8.02 (132)	5.09 (47)		4.36 (26)	5.09 (47)	8.64 (150)	5.49 (59)
				$\tau_1 = 10^{-11}$; $\tau_2 = 1 \times 10^{-6}$; $\tau_r = 1 \times 10^{-12}$						
η	0	−1.0	−1.0	−1.0	−1.0	60	−0.97	−0.96	−0.93	−0.97
r (% error[b])		3.46 (0)	4.05 (17)	6.92 (100)	4.36 (26)		6.93 (100)	8.11 (134)	13.9 (302)	8.74 (152)
η	30	−1.0	−1.0	−1.0	−1.0	90	−1.0	−1.0	−1.0	−1.0
r (% error[b])		4.05 (17)	4.73 (37)	8.09 (134)	5.10 (47)		4.36 (26)	5.10 (47)	8.72 (152)	5.49 (59)
				$\tau_1 = 10^{-11}$; $\tau_2 = 1 \times 10^{-6}$; $\tau_r = 1 \times 10^{-9}$						
η	0	−1.0	−1.0	−0.97	−1.0	60	−0.97	−0.92	−0.32	−0.86
r (% error[b])		3.46 (0)	4.05 (17)	6.93 (100)	4.36 (26)		6.93 (100)	8.09 (134)	13.75 (297)	8.78 (154)
η	30	−1.0	−1.0	−0.93	−1.0	90	−1.0	−1.0	−0.85	−0.99
r (% error[b])		4.05 (17)	4.73 (37)	8.09 (134)	5.10 (47)		4.36 (26)	5.10 (47)	8.78 (154)	5.49 (59)

[a] Other fixed parameters for this calculation are the following: $\omega = 2\pi \times 500$ MHz, $R_s = 0$. [b] r is in Å. Deviation from the distance calculated by using the rigid isotropic model ($r = 3.46$ Å). [c] η would be too small to measure.

formation in Figures 1 and 2 as well as the errors produced when r is evaluated on the basis of the rigid isotropic model. In all cases the initial slope of the cross-peak evolution is a function of *both* the internuclear distance and the angle of internal motional averaging,

The errors reported in Table I are independent of the assumed internuclear distance. The R_C term in eq 4 is a sum of two spectral density functions. Both J factors used to calculate the internuclear distance are products of the r^{-6} term and a term with geometric dependence, the spatial term. When comparing calculated distances with use of the initial slope method, the r^{-6} terms cancel leaving only the spatial terms. Regardless of the value chosen for the reference distance, the same relative prediction of distance is given by the rigid isotropic model and the percent error does not vary.

The initial slopes of the cross-peak evolution depend on angle and τ_r even in the two extreme cases ($\tau_c = 1 \times 10^{-12}$ and $\tau_c = 1 \times 10^{-6}$). For very long correlation times the calculated distances

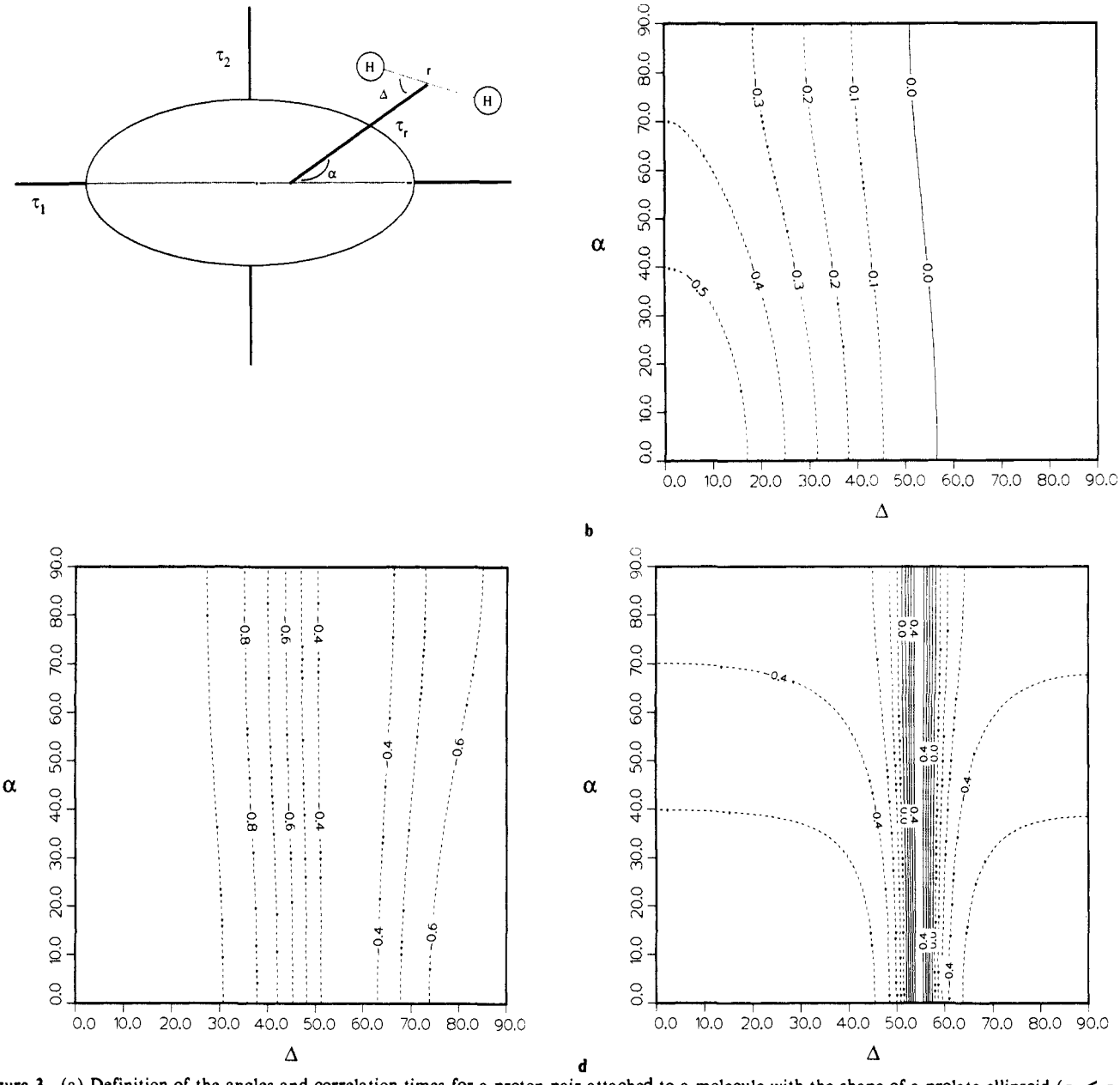

Figure 3. (a) Definition of the angles and correlation times for a proton pair attached to a molecule with the shape of a prolate ellipsoid ($\tau_1 < \tau_2$). The correlation times for the major axis of rotation, the minor axis of rotation, and unrestricted internal rotation of the proton pair, separated by r, are τ_1, τ_2, and τ_r, respectively. The case where $\tau_1 > \tau_2$ represents an oblate ellipsoid. (b–d) NOE enhancements, η, as a function of angles α and Δ for a rotating proton attached to a prolate ellipsoid. Positive enhancements, extreme-narrowing, and negative enhancements, below extreme-narrowing, are represented by solid and dashed lines, respectively. Contour spaces are units of 0.1 η. These plots also apply to two-dimensional cross-relaxation spectra (NOESY) recorded at the optimum mixing time.[14] The cross-peak intensity is obtained by simply reversing the sign of η. (b) $\tau_1 = 5 \times 10^{-10}$, $\tau_2 = 1 \times 10^{-9}$, $\tau_r = 1 \times 10^{-9}$; (c) $\tau_1 = 5 \times 10^{-9}$, $\tau_2 = 1 \times 10^{-8}$, $\tau_r = 1 \times 10^{-9}$; (d) $\tau_1 = 5 \times 10^{-10}$, $\tau_2 = 1 \times 10^{-9}$, $\tau_r = 1 \times 10^{-12}$.

were double the true distance when Δ was near the magic angle (54.7°). When τ_c was given values close to those expected for many biomacromolecules (10^{-8}–10^{-9} s), the ηs and calculated proton–proton distances depended on both the rotational correlation time and the orientation of the rotor. Usually the strongest effects were observed for values of Δ near the magic angle. For most cases, the predicted distances and ηs rose on both sides of the magic angle and then decreased as Δ approached 0° or 90°. The case where τ_c and $\tau_r = 1 \times 10^{-9}$ is noteworthy. The value of η approaches 0 when Δ is greater than or equal to the magic angle yet the predicted distance increased over the same angular range. In contrast, other combinations of τ_c and τ_r give distance errors of approximately 25% as Δ approaches 90°. The combination of numbers for a sphere is important. For a smaller or faster moving sphere ($\tau_c = 1 \times 10^{-12}$), ηs of 0.5 are found regardless of τ_r. The conditions $\tau_c = 1 \times 10^{-9}$ and $\tau_r = 1 \times 10^{-12}$ likewise produce a response similar to that shown in Figure 1. A large or slow moving sphere ($\tau_c = 1 \times 10^{-6}$) is in the spin-diffusion regime. In Figure 1 τ_r values of 1×10^{-9} to 1×10^{-12} yield regions near Δ equal to the magic angle that have $\eta s \neq -1$. The intuitive notion that very slow overall tumbling ($\tau_c = 1 \times 10^{-6}$) will always give enhancements of −1 fails. Even for a case as simple as a sphere with a rotor, conclusions drawn from experimental data where the details of geometry have not been taken into account can be in error.

As previously discussed, the analysis of anisotropic ellipsoids requires the addition of two additional parameters (τ_2 and α) to characterize motional averaging. When comparing the rotations of a sphere to those of a nonspherical ellipsoid, τ_2 for the prolate or oblate ellipse compares directly to τ_c for the sphere. Accordingly τ_2 is more important than τ_1 in the spectral density terms.

Asymmetric biomacromolecules such as proteins, oligosaccharides, and larger DNA/RNA fragments do not deviate greatly from a sphere when the ratio of τ_1 and τ_2 is calculated. Parts b–d of Figure 3 show that the angular dependence of η in prolate ellipsoids is sensitive to relatively small anisotropies in

Table III. Nuclear Overhauser Effect Enhancements and Calculated Interproton Distances for a Rigid Proton Pair Attached to Prolate Ellipsoids[a]

τ_1	τ_2	Δ	η	r (% error[b])
5×10^{-13}	1×10^{-12}	0	0.50	3.46 (0)
		30	0.50	3.52 (2)
		60	0.50	3.63 (4)
		90	0.50	3.67 (6)
5×10^{-10}	1×10^{-9}	0	−0.60	3.46 (0)
		30	−0.54	3.55 (2)
		60	−0.43	3.72 (7)
		90	−0.38	3.80 (10)
5×10^{-9}	1×10^{-8}	0	−0.99	3.46 (0)
		30	−0.99	3.52 (2)
		60	−0.99	3.63 (5)
		90	−0.99	3.67 (6)
5×10^{-7}	1×10^{-6}	0	−1.0	3.46 (0)
		30	−1.0	3.52 (2)
		60	−1.0	3.63 (5)
		90	−1.0	3.67 (6)
1×10^{-9}	1×10^{-6}	0	−1.0	3.46 (0)
		30	−1.0	4.04 (17)
		60	−0.99	6.67 (93)
		90	−1.0	4.36 (26)
1×10^{-11}	1×10^{-6}	0	−1.0	3.46 (0)
		30	−1.0	4.05 (17)
		60	−0.97	6.93 (100)
		90	−1.0	4.36 (26)

[a] Other fixed parameters for this calculation are the following: $\omega = 2\pi \times 500$ MHz, $R_s = 0$. [b] r is in Å. Deviation from the distance calculated by using the rigid isotropic model ($r = 3.46$ Å).

molecular shape (molecular width 80% of molecular length). The correlation times used to generate Figure 3b,c are similar to those found for a slowly rotating proton pair in small proteins, medium sized oligosaccharides, or small DNA/RNA duplexes. The angular dependence of η is similar to that of the corresponding sphere with internal motion. The α dependence is small. Figure 3b demonstrates that the critical correlation time (when $\eta = 0$) can be highly dependent on Δ. As τ_1 and τ_2 approach the inverse of the spectrometer frequency and τ_r is small (fast internal rotation), the α dependence increases (Figure 3d). In addition there is a magic-angle effect for Δ. For a much larger molecule spin diffusion ($\tau_2 \cong 1 \times 10^{-6}$ to 1×10^{-7}) will dominate. The magic angle effect for Δ is manifested over only a 6° range of angles (52° through 58°). Otherwise η approaches a value of −1 (see supplementary material). In very large molecules faster internal rotation of the proton pair narrows the range of the magic angle effect even more (see supplementary material). The magic angle effect for Δ becomes smaller as τ_1 and τ_2 become larger.

The corresponding distance errors for prolate ellipsoids calculated with eq 4 can be found in Table II. For prolate ellipsoids the distances calculated with the standard assumptions are always longer than the actual distance. It is worth noting that the calculated distance can be in error by very large amounts even in cases where the value found for η is close to that predicted by the rigid isotropic model. This is shown graphically in the supplementary material. When τ_1 and τ_2 are large (spin-diffusion), the slopes still depend on α and Δ. However, the calculated internuclear distance assuming the rigid isotropic model is insensitive to the internal correlation time, τ_r. As was observed in Figure 2a, for long correlation times the initial slope is linear over only a very short range of mixing times. Additional plots of cross-peak evolution for other types of prolate ellipsoids are in the supplementary material.

The angular dependence of η for oblate ellipsoids where $\tau_1 \approx \tau_2$ is similar to the prolate case except for reversal of the contour curvature about the α axis (see supplementary material). The errors in the calculated internuclear distance are listed in a table in the supplementary material. The errors are similar in magnitude to those found for prolate ellipsoids but the patterns are different. The order of the angular dependence of the slopes has changed. Graphs of the cross-peak evolution for oblate ellipsoids are in the supplementary material. Except for when Δ is close to 0, the

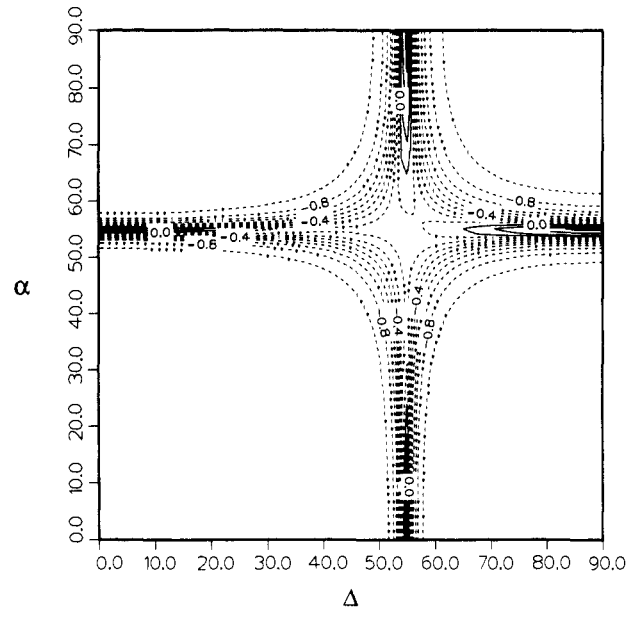

Figure 4. NOE enhancements, η, as a function of angles α and Δ for a rotating proton attached to a highly anisotropic prolate ellipsoid. Positive enhancements, extreme-narrowing, and negative enhancements, below extreme-narrowing, are represented by solid and dashed lines, respectively. Contour spaces are units of 0.1 η. These plots also apply to two-dimensional cross-relaxation spectra (NOESY) recorded at the optimum mixing time.[14] The cross-peak intensity is obtained by simply reversing the sign of η. $\tau_1 = 1 \times 10^{-11}$, $\tau_2 = 1 \times 10^{-6}$, $\tau_r = 1 \times 10^{-9}$.

distances predicted by the rigid isotropic model are found to be too long.

Molecules in phospholipid bilayers, micelle components, and a variety of semiflexible polymer systems studied in the material sciences undergo far more anisotropic averaging than do proteins. Figure 4 contains the angular dependence of η for an anisotropic, prolate ellipsoid. The results indicate there is a strong dependence of η upon α and Δ for molecules with highly anisotropic motional averaging. The magic angle effect, which is present for both angles of rotation, is important over a wide range of angles when internal rotation is slow. As the rotation about the major axis of the ellipsoid decreases, the range of the magic angle effect is somewhat diminished (plots shown in the supplementary material). The value of η observed when α or Δ is in this range would be misinterpreted as a smaller enhancement or a weaker cross-peak under the conventional, rigid isotropic rotor assumption. Anisotropic molecules have the largest dependency of their initial slope of the cross-peak evolution on α and Δ. Furthermore, many of the curves overlap making an unambiguous interpretation with measurements at a single magnetic field strength impossible (see supplementary material). The errors in r as measured by cross-peak evolution are tabulated in Table II. The distance errors are very large (300%) near the magic angle. Only when α and Δ are both near 0° do the distance errors fall below 20%.

Highly anisotropic oblate ellipsoids represent macromolecules with the shape of a thin disk. To gain insight into the cross-relaxation behavior for this class of molecules, the angular dependence of η was calculated (see supplementary material). The angular dependence is much different than that for prolate ellipsoids. There is no sensitivity to the magic angle, but the observed η is sensitive to the value of Δ and relatively insensitive to α. When $\tau_1 = 1 \times 10^{-6}$, $\tau_2 = 1 \times 10^{-9}$, $\tau_r = 1 \times 10^{-9}$, the value of η drops by a factor of 4 as Δ goes from 30° to 60°. A table in the supplementary material contains the results of cross-peak evolution calculations for oblate ellipsoids. The predicted distances for oblate ellipsoids exhibit greater errors for slower internal motion. The errors change from overestimates to underestimates as the proton pair's internal motion decreases and as the degree of anisotropy increases. Graphs of the cross-peak evolution of oblate ellipsoids with slow and fast internal motion are also deposited in the supplementary material. The initial slopes vary more with in-

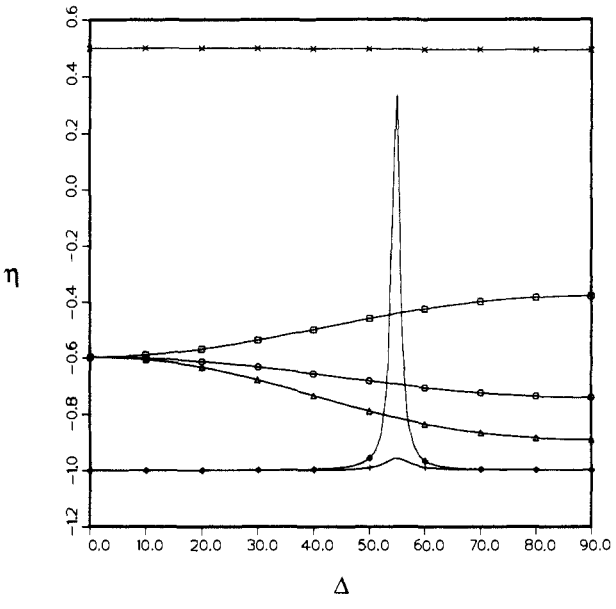

Figure 5. NOE enhancements, η, as a function of the angle Δ for a fixed proton pair attached to prolate and oblate ellipsoids: (□) $\tau_1 = 5 \times 10^{-10}$, $\tau_2 = 1 \times 10^{-9}$; (○) $\tau_1 = 2 \times 10^{-9}$, $\tau_2 = 1 \times 10^{-9}$;; (△) $\tau_1 = 1 \times 10^{-6}$, $\tau_2 = 1 \times 10^{-9}$; (+) $\tau_1 = 1 \times 10^{-9}$, $\tau_2 = 1 \times 10^{-6}$; (×) $\tau_1 = 1 \times 10^{-6}$, $\tau_2 = 1 \times 10^{-11}$; (◇) $\tau_1 = 1 \times 10^{-11}$, $\tau_2 = 1 \times 10^{-6}$.

creased internal rotation relative to the prolate case.

Case 2: Ellipsoids with No Internal Rotation. When the two protons are rigidly attached to the surface of a sphere, the motion of the protons is perfectly isotropic. In fact, this is the widely used rigid isotropic model for calculating the spectral density functions. There is no angular dependence for cross-relaxation in this case. Both η and the rate of cross-peak evolution depend only upon a single correlation time and the internuclear distance.

A rigid proton pair in a prolate ellipsoid is a simple model for protons in the backbone of a peptide, for amide N–H protons in a β-sheet assembly, and for protons in DNA/RNA fragments. When the proton pair is rigid, the angle α has no meaning (see eq 5). Figure 5 illustrates the dependence of η on Δ for both prolate ($\tau_1 < \tau_2$) and oblate ($\tau_1 > \tau_2$) ellipsoids. Near the magic angle the calculated η deviates significantly from the value predicted by the rigid isotropic model. For highly anisotropic, prolate ellipsoids where τ_2 is well into the spin-diffusion domain ($\tau_2 \approx 1 \times 10^{-6}$), the magic angle effects are particularly strong. In Figure 5 both cases where $\tau_2 = 1 \times 10^{-6}$ generate ηs near −1 except when Δ is near the magic angle. The maximum at the magic angle is higher for smaller τ_1 values. For anisotropic, prolate ellipsoids the calculated η deviates significantly from the value predicted by the rigid isotropic model when Δ is near the magic angle. As the motion about the major axis (τ_1) slows, the range of the magic angle effect is reduced. The angular dependence for the initial slope of cross-peak evolution can be found in Table III. In contrast to the case with internal rotation, the errors in evaluating the internuclear distance are quite small when $\tau_1 \approx \tau_2$. Significant errors are encountered only for highly anisotropic molecules. As long as the deviation from spherical symmetry is modest, the calculated distances will be accurate. This accounts for the successful application of the single correlation time model in determining distance constraints for rigid portions of biomacromolecules.

The dependence of η on Δ for a rigid proton pair in oblate ellipsoids can also be found in Figure 5. The results are markedly different from those obtained for prolate ellipsoids. There is no magic angle dependence. Since τ_2 dominates the spectral density functions, τ_2 also dominates the determination of η. This leads to the surprising predicted value for η of 0.5 when τ_1 is well into the spin-diffusion regime (1×10^{-6}) but τ_2 is short (1×10^{-11}). The angular dependence of the cross-peak evolution is also different than that for prolate ellipsoids. Figures that portray the cross-peak evolution curves for anisotropic oblate ellipsoids can be found in the supplementary material. The value of τ_2 also dominates the slopes of the cross-peak evolution. Errors in internuclear distance measurements using the rigid isotropic rotor model are small for a wide variety of τ_1, τ_2 combinations.

Discussion

The primary conclusion of this investigation is that homonuclear proton cross-relaxation is not necessarily dominated by the internuclear distance. The results show that the shape of the molecule, orientation, and rate of internal rotation for the rotating pair can be important factors. The implications of these calculations deserve some discussion. In general the enhancements are less sensitive to orientation than is the growth of cross-peak intensity. The calculation of η requires taking the quotient of two quantities, the cross-relaxation in the numerator and the leakage terms in the denominator. When external relaxation is set to 0, the r^{-6} term that multiplies the spectral density functions cancels. The only portions of the spectral density functions that remain in the calculation of η are the spatial terms. Regardless of the value of r, the geometric arrangement of the proton pair determines the value of η for a given set of correlation times. By contrast cross-peak evolution, like T_1 and T_2, is a rate process. In the limits of the rigid isotropic approximation, the rate of change of cross-peak intensity depends only upon distance and a single correlation time. When the full expression for the spectral density functions is used, the spatial factors become important. Unlike the calculation for the enhancement, which involves quotients, cross-peak evolution depends on sums of spectral density functions. Terms involving spatial factors do not cancel, and these factors are even more important when calculating the cross-peak time dependence.

For small molecules, which are well into the extreme-narrowing regime, the rigid isotropic assumption is valid except when Δ exceeds 55°. Even when Δ has values larger than 55° the errors in calculating r are barely larger than the reproducibility of the experimental technique. It is likely that difficulties encountered in stimulating experimental cross-relaxation data would result from ignoring the importance of cross-correlated spectral densities. In macromolecules, molecular shape and internal motion must be considered in the interpretation and simulation of experimental results. Fitting experimental cross-relaxation data to theoretical results as a function of correlation time alone is not justified. When internuclear distances are determined, the slope of the cross-peak evolution for a well-characterized proton pair is often used to calibrate internuclear distances. This calculation is usually done assuming a single correlation time. Our results indicate that such calibrations are not exact, except for a sphere with no internal motion. In all other cases, corrections should be applied for the shape of the molecule, the orientation of the pair, and the rate of internal motion. Fortunately, calibrations for rigid protons in molecules approximating the shape of a sphere will have errors on the order of current experimental inaccuracies. Pairs whose internuclear distances are to be calculated on the basis of the calibration will need to have similar corrections for shape, orientation, and internal motion. Side chains of proteins or other portions of macromolecules that have free rotation will be best evaluated by using the full equations for the spectral density functions presented here. Several representative calibrations for various types of proton pair geometries in a molecule may prove useful. For instance, the symmetry properties of the DNA helix would make multiple calibrations attractive for refining distance constraints in large DNA/RNA fragments. Similar symmetry considerations inherent in amino acid helices and β-sheet structures would also be worth exploration when quantitative simulation of experimental cross-relaxation experiments fails.

Qualitative conclusions are also compromised when geometrical factors and internal motion are not considered. The use of general categories of strong, medium, or weak cross-peaks to qualitatively rank distances can be unreliable. Cases were presented in which nuclear Overhauser enhancements completely disappear depending on orientation and shape and rate of internal motion. Likewise, the characterization of behavior as being extreme-narrowing or

spin-diffusion becomes meaningless as each pair of protons may exhibit either behavior or behavior between the extremes. The relative sign of a cross-peak will not necessarily accurately reflect the rate of global molecular reorientation. Extreme-narrowing (anti-phase with respect to the diagonal) cross-peaks observed in NOESY spectra of macromolecules should not be ignored or automatically assigned to artifacts. The simulations show that motional averaging about an angle in the range of 50° to 60° will produce this type of cross-peak. Indeed, confirmation of a negative cross-peak would yield a new structural constraint. A spatial constraint would define a range of angles for the orientation of motional averaging of a proton pair with respect to the major axis of global molecular reorientation.

The calculations indicate that highly anisotropic molecular orientation will produce results that cannot be explained by calculations on the basis of the rigid isotropic assumptions. Oriented molecules in lipid bilayers and micelles or semiflexible polymers encountered in material sciences demand application of the full spectral density functions. In extremely high magnetic fields (^{1}H frequencies >500 MHz) molecules with large dipole moments are known to align along the direction of the static field. The results for highly anisotropic motion ($\tau_1 \ll \tau_2$) would become important under these circumstances.

While we have only considered isolated spin pairs, the spatial aspects of spin topology and internal motion will be important for understanding cross-relaxation in multiple-spin relaxation networks. Multiple-spin networks, including the effects cross-correlated spectral densities, are now under investigation in our laboratories.

Supplementary Material Available: An Appendix describing the theoretical section in more detail, additional plots of the angular dependence of η, the NOESY cross-peak evolution for a variety of molecular sizes and shapes, and tables containing calculations of η and distance errors for oblate ellipsoids (47 pages). Ordering information is given on any current masthead page.

Tl^I–Tl^I and In^I–In^I Interactions. From the Molecular to the Solid State

Christoph Janiak and Roald Hoffmann*

Contribution from the Department of Chemistry and Materials Science Center, Cornell University, Ithaca, New York 14853. *Received November 6, 1989*

Abstract: The influence of the ligand geometry on Tl^I–Tl^I and In^I–In^I bonding has been studied within the extended Hückel framework, looking at the following observed molecular and solid-state structures or structural types (respective metal moiety given in parentheses): $\{(PhCH_2)_5C_5Tl/In\}_2$ (dimer), $\{TlOMe\}_4$ (bridged tetramer), $Tl_2Te_2^{2-}$ (bridged dimer), $\{Me_5C_5In\}_6$ (octahedral hexamer), $\{MeC_5H_4In\}_\infty$ (dimers), TlS = $Tl^ITl^{III}S_2$ (TlSe-type, linear chains), $In_{11}Mo_{40}O_{62}$ (chain segments), $InMo_4O_6$ (linear chain), and $TlCo_2S_2$ ($ThCr_2Si_2$-type, square-planar nets). For Tl^I and In^I complexes with large Tl^I···Tl^I and In^I···In^I separations the ligand environment (especially the L–M–M angle) is found to be the dominant factor in determining the extent of the bonding interaction between the metals. The metal–metal distances in these compounds range from about 265 to 400 pm. We have interpreted the metal–metal interaction in these systems with the help of model complexes, such as Tl_2, Tl_2H_2, $\{C_5H_5Tl/In\}_2$, $\{TlOMe\}_2$, $\{HIn\}_6$, $\{C_5H_5In\}_6$, Tl/In_∞, $\{TlH_4/S_4\}_\infty$, $\{InO_4\}_\infty$, Tl_{nets}, and $\{TlH_4/S_4\}_{nets}$ with the ligands in various geometrical arrangements. Starting the analysis with a bare Tl_2 dimer or Tl_∞ chain, it is shown that a mixing of empty p levels into the filled s combinations is the basis for a bonding interaction. The behavior of the overlap population as a function of the ligand geometry is then studied. A detailed angle variation in Tl_2H_2 helped us to understand why one passes from an almost nonbonding situation in the linear arrangement, over a region of strong bonding upon trans-bending of the hydrogens, to again reach a nonbonding interaction in the bridging geometry. What happens in the trans-bending in Tl_2H_2 is closely related to the orbital interactions in the pyramidalization of AH_3 systems (e.g. NH_3) and the bending of AH_2 molecules (e.g. H_2O). Calculations on the more realistic examples $\{TlOMe\}_2$, $\{C_5H_5Tl/In\}_2$, and $Tl_2Te_2^{2-}$ confirmed that a trans-bent geometry with a ligand–M–M angle close to 120° gives an optimum overlap population at a relatively long, fixed Tl^I–Tl^I or In^I–In^I separation in molecular systems. A bridging ligand geometry, either in a molecular complex or in an extended structure, generally gave a non- or antibonding metal–metal overlap population. This is in agreement with the apparent general consensus in the literature that the bridged species do not display any Tl–Tl interactions. Dimers where the trans-bent geometry has been observed, despite their long M–M contacts (such as 363 pm as in $\{(PhCH_2)_5C_5Tl/In\}_2$), can be assigned a definite M^I–M^I bonding interaction. The bonding in solid-state structures with Tl^I–Tl^I or In^I–In^I contacts was analyzed with the help of band structure diagrams, density of state, and crystal orbital overlap population plots. A prior look at the interaction in a (molecular) Tl_2 dimer in a square-pyramidal or cubic ligand field facilitated the interpretation. Extended structures showed an optimum at ligand–M–M angles of 90°, resulting in a square-planar ligand field for metal chains or an on-top/bottom position in metal nets. While a square-planar ligand field increases the s–p_z mixing, hence overlap population, with respect to the bare Tl/In chain or net, a cubic ligand environment widens the s–p_z energy gap, thereby decreasing mixing and overlap population.

Introduction

With this paper we provide some material for a discussion of thallium(I)–thallium(I) and indium(I)–indium(I) interactions whose tendencies to form unusual contacts cannot be overlooked, yet whose bonding character remains mostly unclear. We will carry out our theoretical study on the basis of the very simple, semiempirical, extended Hückel formalism. We are aware of its limitations: It is a one-electron model with no spin–orbit coupling, no configuration interaction. Relativistic effects, likely to be important for heavy atoms, are not accounted for explicitly, only in our choice of parameters (which may be problematic in itself). We also cannot satisfactorily optimize most structures. But we are certain that within our model we can develop a chemical understanding, an analysis of those structural types in which Tl^I–Tl^I and In^I–In^I bonding interactions are likely to be present.

Of course, the problems discussed here are related to the larger question of stereochemical activity of a lone pair in compounds of elements that have an s^2 configuration.[1]

0002-7863/90/1512-5924$02.50/0